

Supporting Information

Electronic and Optical Properties of Pristine and Vertical and Lateral

Heterostructures of Janus MoSSe and WSSe

Fengping Li, Wei Wei,^{*} Pei Zhao, Baibiao Huang, Ying Dai^{*}

School of Physics, State Key Laboratory of Crystal Materials, Shandong University,

Jinan 250100, China

Corresponding Author: wei@sdu.edu.cn, (W. Wei) daiy60@sdu.edu.cn (Y. Dai)

COMPUTATIONAL DETAILS

The first-principles calculations were performed on the basis of density functional theory (DFT) as implemented in the Vienna Ab Initio Simulation Package (VASP).^{1,2} The electron exchange correlation was treated with the Perdew–Burke–Ernzerhof (PBE) in the framework of generalized gradient approximation (GGA).³ The DFT Kohn-Sham equations were resolved by the projector augmented wave (PAW) through the plane wave basis set. The cutoff energy of 500 eV was chosen for plane-wave expansion of wave functions and Monkhorst–Pack (MP) scheme for k-point sampling was employed for the integration over the first Brillouin zone.⁴ The $13 \times 13 \times 1$ k-point mesh was used for 1×1 MoSSe/ 1×1 WSSe VHTs cells, while $7 \times 7 \times 1$ k-point was employed for LHTs with $n=3, 4, 5, 6, 7, 8, 9$. Structures were relaxed until the atomic forces on each ionic were less than 0.01 eV/\AA^{-1} and the electron relaxation convergence criterion was 10^{-4} eV in two consecutive loops. In order to mimic the isolated layers, a vacuum space was set to 25 \AA . In addition, the state of art many-body calculations were conducted to obtain the quasiparticle electronic features, in which the enhanced e - e interactions were included.⁵ The quasiparticle energies from single shot G_0W_0 were adopted to obtain the band structures by Wannier interpolation through the Wannier90 program.⁶ Besides, Bethe-Salpeter equation (BSE) in consideration of e - h interactions was resolved to address the optical absorption based on the G_0W_0 results. For comparison, Heyd–Scuseria–Ernzerhof (HSE06) hybrid functional that includes nonlocal exchange effects was adopted.⁷ In order to consider the vdW interactions for the VHTs, DFT-D2 corrections within the PBE

functional were performed to give more accurate results.⁸ The dipole corrections perpendicular to the interfaces of VHTs were considered.⁹ Furthermore, *ab initio* Born–Oppenheimer molecular dynamics (BOMD) simulations were conducted to evaluate thermal stability of LHTs at 300 K for 3000 fs with a time step of 1 fs.¹⁰ Additionally, the photo-response was calculated with the Keldysh nonequilibrium Green’s functions (NEGF-DFT).¹¹ A double-zeta polarized (DZP) atomic orbital basis was used for NEGF-DFT calculations to expand all the physical quantities. The exchange and correlation were treated at the level of the local density approximation (LDA) and atomic cores are defined by the standard norm conserving nonlocal pseudopotentials. The total Hamiltonian is expressed by:

$$\hat{H} = \hat{H}_0 + \frac{e}{m_0} \hat{A} \cdot \hat{P}$$

where \hat{H}_0 , \hat{A} and \hat{P} are the self-consistent Hamiltonian of the system, electromagnetic vector potential and the momentum of the electrode, respectively.

REFERENCES

- (1) Kresse, G.; Joubert, D. From Ultrasoft Pseudopotentials to the Projector Augmented-Wave Method. *Phys. Rev. B* **1999**, *59*, 1758–1774.
- (2) Kresse, G.; Furthmuller, J. Efficient Iterative Schemes for Ab Initio Total–Energy Calculations Using a Plane–Wave Basis Set. *Phys. Rev. B: Condens. Matter Mater. Phys.* **1996**, *54*, 11169.
- (3) Perdew, J. P.; Burke, K.; Ernzerhof, M., Generalized Gradient Approximation Made Simple. *Phys. Rev. Lett.* **1996**, *77*, 3865–3868.

- (4) Monkhorst, H. J.; Pack, J. D. Special Points for Brillouin-zone Integrations. *Phys. Rev. B* **1976**, 13, 5188–5192.
- (5) Shishkin, M.; Kresse, G. Implementation and Performance of the Frequency-Dependent GW Method within the PAW Framework. *Phys. Rev. B* **2006**, 74, 035101.
- (6) Mostofi, A. A.; Yates, J. R.; Lee, Y.-S.; Souza, I.; Vanderbilt, D.; Marzari, N. wannier90: A tool for Obtaining Maximally-Localized Wannier Functions. *Comput. Phys. Commun.* **2008**, 178, 685–699.
- (7) Krukau, A. V.; Vydrov, O. A.; Izmaylov, A. F.; Scuseria, G. E. Influence of the Exchange Screening Parameter on the Performance of Screened Hybrid Functionals. *J. Chem. Phys.* **2006**, 125, 224106.
- (8) Grimme, S. Semiempirical GGA-type Density Functional Constructed with a Long-range Dispersion Correction. *J. Comput. Chem.* **2006**, 27, 1787–1799.
- (9) Makov, G.; Payne, M. C. Periodic Boundary Conditions in ab initio Calculations. *Phys. Rev. B* **1995**, 51, 4014–4022.
- (10) Barnett, R. N.; Landman, U. Born-Oppenheimer Molecular-dynamics Simulations of Finite Systems: Structure and Dynamics of (H₂O)₂. *Phys. Rev. B* **1993**, 48, 2081–2097.
- (11) Waldron, D.; Haney, P.; Larade, B.; MacDonald, A.; Guo, H. Nonlinear Spin Current and Magnetoresistance of Molecular Tunnel Junctions. *Phys. Rev. Lett.* **2006**, 96, 166804.

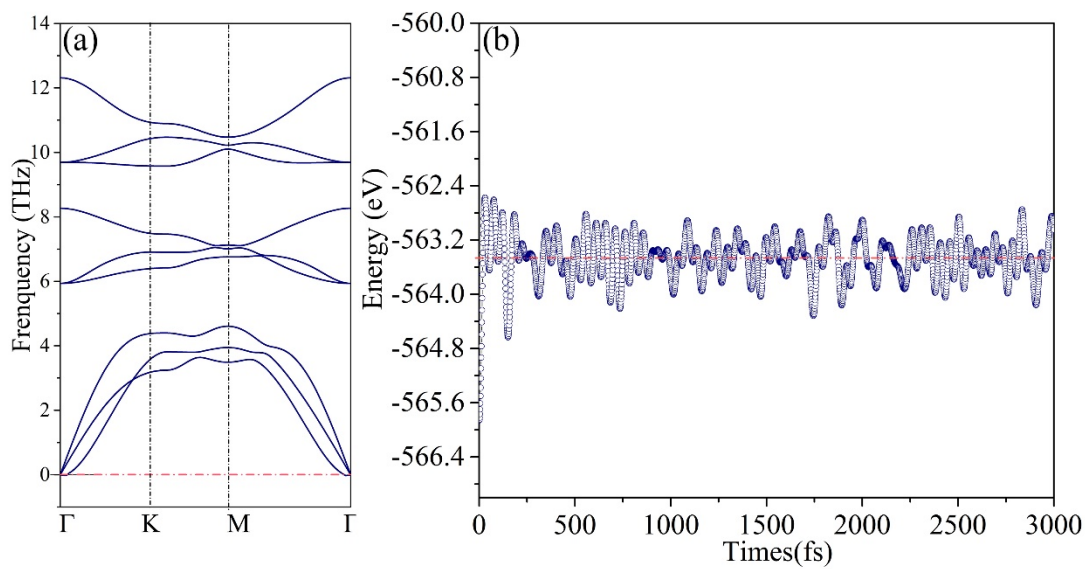


Figure S1 The phonon spectrum (a) and the variation of free energy by BOMD at 300 K during the timescale of 3000 fs (b) for MoSSe.

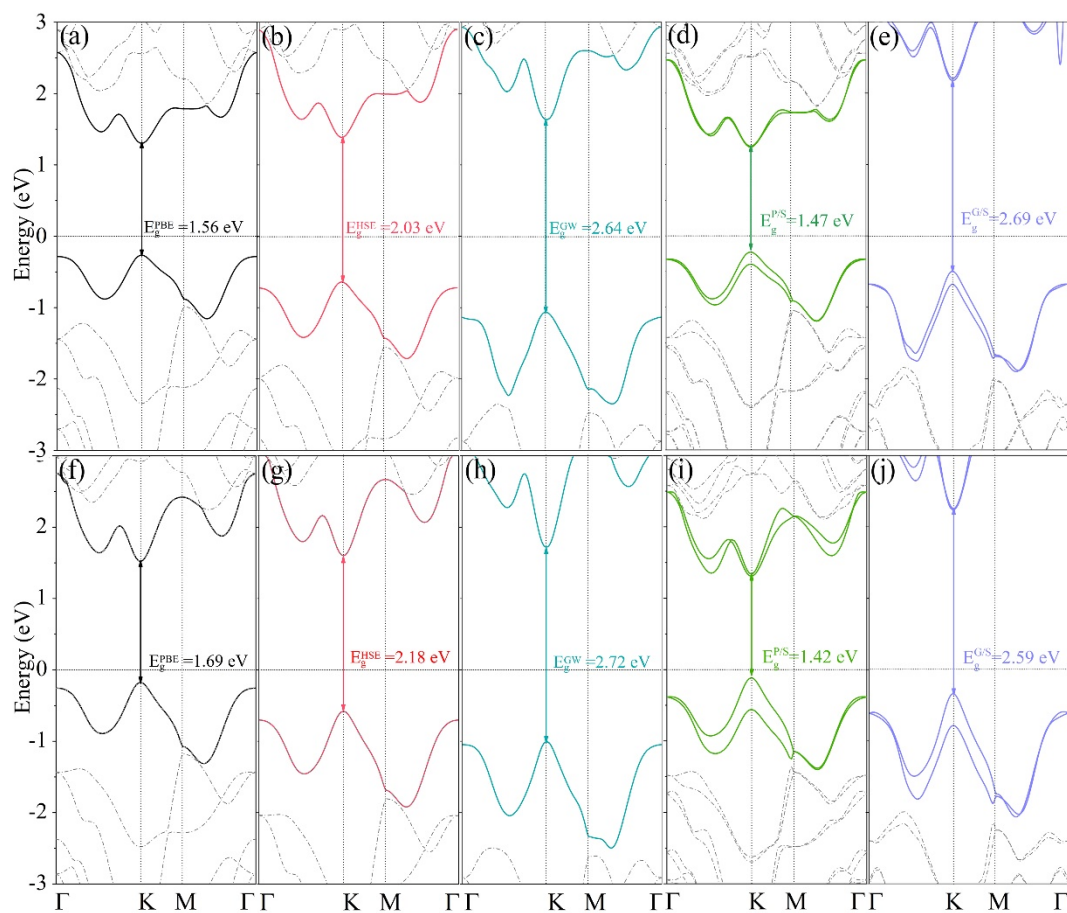


Figure S2 Band structures of MoSSe from PBE (a), HSE06 (b), G_0W_0 (c), PBE+SOC (d) and G_0W_0 +SOC (e). Band structures of WSSe from PBE (f), HSE06 (g), G_0W_0 (h), PBE+SOC (i) and G_0W_0 +SOC (j). The Fermi level is set to zero.

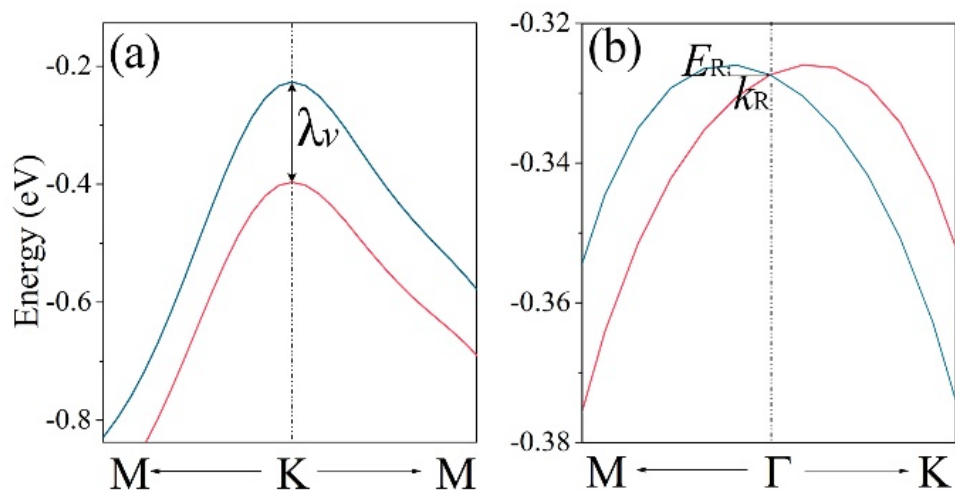


Figure S3 The amplified band structure of MoSSe around the K and Γ points, which represent the out-of-plane (a) and in-plane spin polarization (b). Blue and red indicate spin up and spin down.

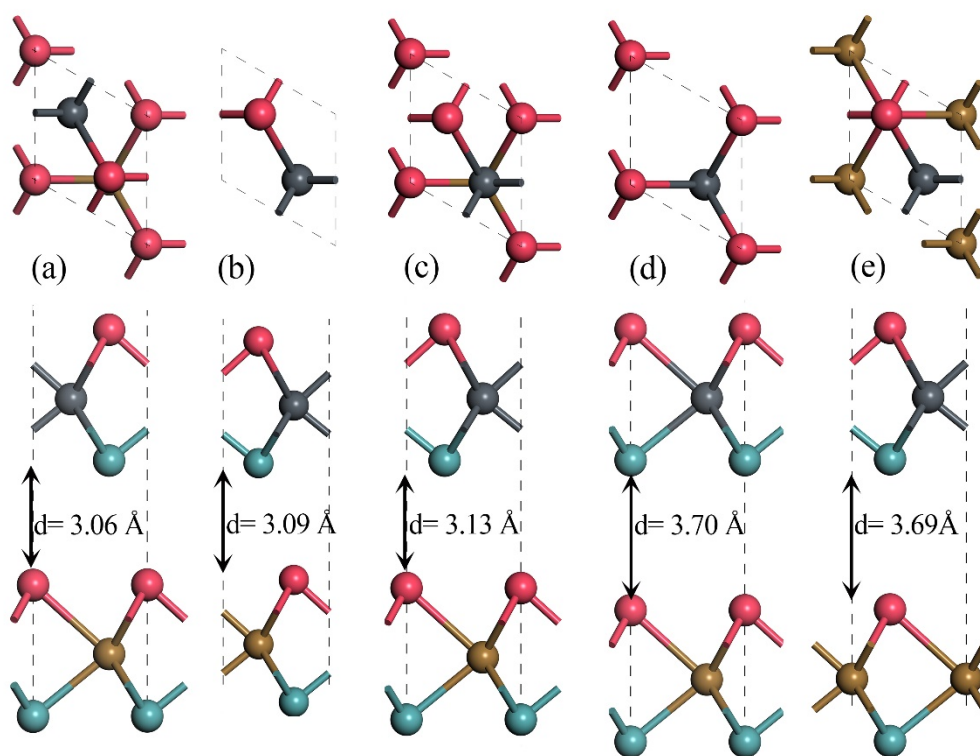


Figure S4 Top and side views of high symmetry stacking model of AB (a), AA' (b), AB' (c), AA (d) and A'B (e) for the VTHs, and the interlayer distances are labeled.

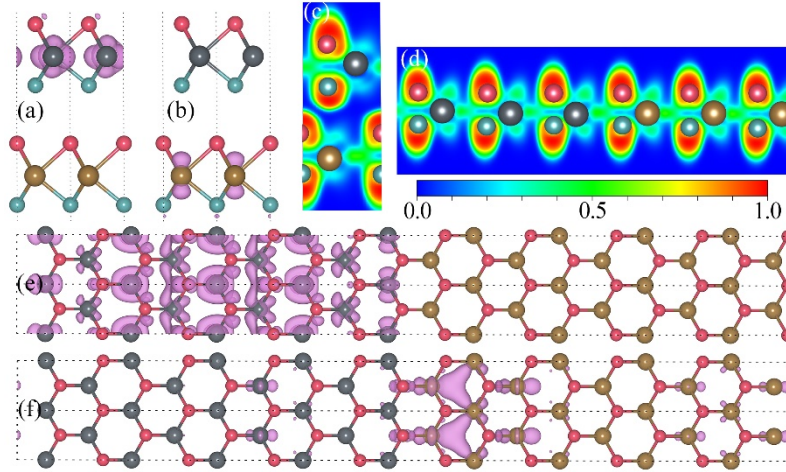


Figure S5 Charge density of CBM (a) and VBM (b) for VTHs. Electron localization functions (ELFs) for VTHs (c) and LTHs (d). Charge density distribution of CBM (e) and VBM (f) for LTHs.

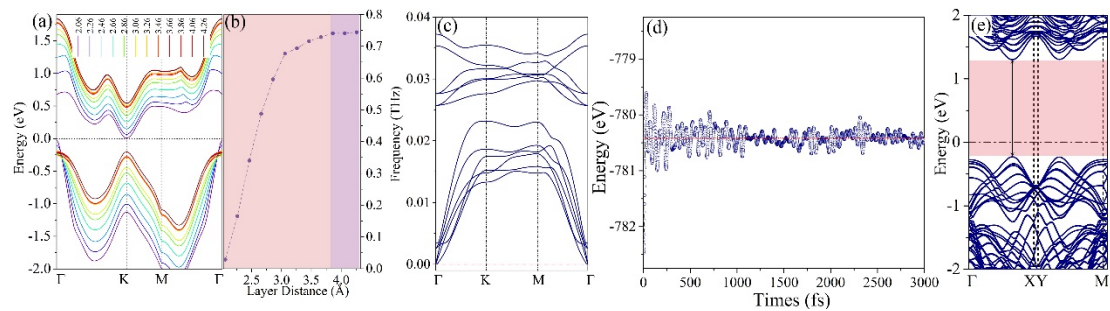


Figure S6 Band edge (a) and band gap (b) for VHTs as interlayer distance changes. Phonon spectrum for VHTs (c). Variation of free energy for LHTs ($n=9$) by BOMD at 300 K during the timescale of 3000 fs (d). Band structure of the LHTs ($n=9$) along the Γ -X-Y-M (e), the Fermi level is set to zero.

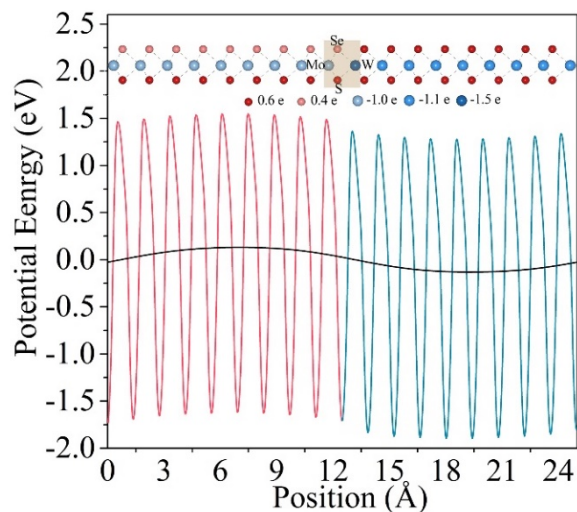


Figure S7 Planar average of the electrostatic potential energy along the direction perpendicular to the interface for LHTs ($n=9$), and the macroscopic average of the electrostatic potential energy (black line) is also shown. Inset shows the net charge distribution for LHTs ($n=9$) from Bader charge calculation. The brown rectangle represents the interface region. Red and blue balls depict the charge accumulation and depletion, respectively, and the corresponding values are labeled.

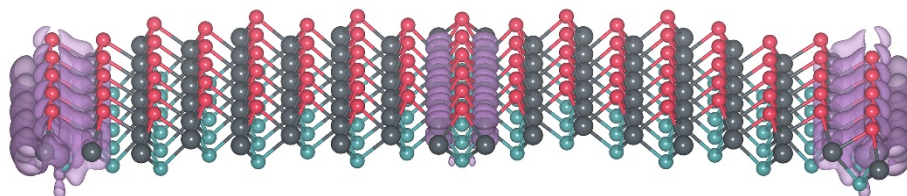


Figure S8 Charge density distribution of 60° GBs for MoSSe ($n=9$).